Cheng, L., Cord-Ruwisch, R. and Shahin, M. A. (2013) Cementation of sand soil by microbially induced calcite precipitation at various degrees of saturation. Canadian Geotechnical Journal, 50 (1). pp. 81-90.

Cementation of Sand Soil by Microbially Induced Calcite Precipitation at Various Degrees of Saturation

Liang Cheng[1], Ralf Cord-Ruwisch[2], Mohamed A. Shahin[3]

[1]Liang CHENG: Ph.D. student, School of Biological Sciences and Biotechnology, Murdoch University, South Street, Murdoch, Western Australia, 6150, Australia. Email: L.Cheng@murdoch.edu.au

[2]Ralf Cord-Ruwisch: Senior Lecturer, School of Biological Sciences and Biotechnology, Murdoch University, South Street, Murdoch, Western Australia, 6150, Australia. Email: R.Cord-Ruwisch@murdoch.edu.au

[3]Mohamed A. Shahin: Associate Professor, Department of Civil Engineering, Curtin University, Perth WA, 6845, Australia. Email: M.Shahin@curtin.edu.au

Corresponding author: Liang CHENG: Ph.D. student, School of Biological Sciences and Biotechnology, south street campus, Murdoch University, 90 South Street, Murdoch, Western Australia, 6150, Australia. Email: L.Cheng@murdoch.edu.au & c_howking@hotmail.com Tel: +61-8-93602403; Fax: +61-8-93107084;

Submitted to: **Canadian Geotechnical Journal**

Cementation of Sand Soil by Microbially Induced Calcite Precipitation at Various Saturation Degrees

Liang Cheng, Ralf Cord-Ruwisch, Mohamed A. Shahin

Abstract:

A newly emerging microbiological soil stabilization method, known as microbially induced calcite precipitation (MICP), is tested for geotechnical engineering applications. MICP is a promising technique that utilizes the metabolic pathways of bacteria to form calcite precipitation throughout the soil matrix, leading to an increase in soil strength and stiffness. This paper investigates the geotechnical properties of a sand bio-cemented under different degrees of saturation. A series of laboratory experiments was conducted, including sieve analysis, permeability, unconfined compressive strength, consolidated undrained triaxial, and durability tests. The results indicate that higher soil strength can be obtained at similar $CaCO_3$ content when the treatment is performed under low degree of saturation. Fine sand samples exhibited higher cohesion but lower friction angle than coarse sand samples with similar $CaCO_3$ content. The results also confirm the potential of MICP as a viable alternative technique for soil improvement in many geotechnical engineering applications, including liquefiable sand deposits, slope stabilization and subgrade reinforcement. The freeze thaw and acid rain resistance of MICP treated sand has also been tested.

CE Database keywords: Soil stabilization; Cementation; Microorganisms; Calcium carbonate; Durability.

1 Introduction

Current soil improvement applications include soil replacement, preloading for achieving consolidation, chemical admixture and grouting stabilization. These techniques are time consuming, expensive and in the case of grouting and admixture stabilization are environmentally detrimental (DeJong et al. 2010). In 1974 in Japan a case study documented by Karol (2003) illustrated the environmental impact when acrylamide grout leached into waterways causing five substantiated cases of water poisoning. As a result a ban was placed on nearly all chemical grouts, further reverberating to other countries to apply similar prohibition (Karol 2003). Therefore, continuing studies into finding alternative soil improvement methods are vital to achieve optimum performance, economic viability and environmental sustainability.

Calcite *in-situ* precipitation system (CIPS) and microbially induced calcite precipitation (MICP) have been the subjects of research for several industrial applications. Improvement of soil mechanical properties by MICP is currently of particular interest to engineers and microbiologists, and has been demonstrated by several researchers at varying scales (DeJong et al. 2006; Whiffin et al. 2007; van Paassen et al. 2010). The technique can alter the soil characteristics to increase the shear strength and stiffness, while maintaining adequate permeability (Burbank et al. 2011). The technique involves introducing aerobically cultivated bacteria with highly active urease enzyme into soil, harnessing the urease enzyme to catalyze the hydrolysis of urea to produce ammonium and carbonate ions. The chemical reaction involved in this process is shown as follows (Eq. 1):

[1] $CO(NH_2)_2 + 2H_2O \rightarrow 2NH_4^+ + CO_3^{2-}$

In the presence of an introduced calcium source, often calcium chloride ($CaCl_2$), the calcium carbonate ($CaCO_3$, calcite) forms throughout the soil matrix based on the following chemical reaction (Eq. 2):

[2] $Ca^{2+} + CO_3^{2-} \rightarrow CaCO_3$ (s)

The produced microbially induced $CaCO_3$ precipitates bridge adjacent soil particles by cementing the soil grains together to form cemented sand illustrative of calcareous rock (DeJong et al. 2006).

Controlling the MICP process and predicting the resulting material properties are essential in improving the engineering properties of porous solid materials (e.g. soil). Many researchers have investigated the empirical correlations between the amount of precipitated $CaCO_3$ crystals and soil engineering parameters such as the soil porosity, strength, stiffness and permeability (Ismail et al. 2002a, 2002b; Whiffin et al. 2007). The initial properties of soils and the precipitated $CaCO_3$ crystals can vary in mineral type, density, shape, size distribution and texture (Mitchell and Ferris 2006; Ismail et al. 2002a; Warren et al. 2001), which might give an explanation for the observed differences in the resulting engineering properties of MICP treated soils.

In a previous study carried out by Cheng and Cord-Ruwisch (2012), more effective crystals precipitating at the sand particles contact points were achieved under a low degree of saturation. This suggested that by controlling the *in-situ* saturation conditions during the MICP process, the distribution of crystals can be predominantly controlled

and restricted to the inter-particle contact points. In the current paper, the feasibility of MICP as a promising ground improvement technique is evaluated via a series of laboratory tests using sand columns under various saturation conditions. The laboratory results demonstrate the potential of this technique for geotechnical engineering applications such as preventing liquefaction and improving the stability of embankments.

2 Materials and Testing Methods

2.1 Sand Soil Tested

Two different types of pure silica sand (Cook Industrial, Minerals Pty. Ltd. Western Australia) were selected for the current study. Sieve analysis was performed for both fine and coarse grained sands to determine the particle size distribution, which is one of the primary components that govern the mechanical behavior of soils. The particle size distribution curves of the fine and coarse sands used are shown in Figure 1. Both sands are classified as poorly graded sand according to the Unified Soil Classification System (USCS). Poorly graded sands were selected as they exhibit undesirable engineering behavior for most geotechnical engineering applications. Both sands have a specific gravity of 2.62.

2.2 Bacterial Suspension and Cementation Solution for MICP System

The urease active strain of *Bacillus sphaericus* (MCP-11) (DSM 23526, available now from DSMZ, Germany), which was isolated from the previous study (AI-Thawadi and Cord-Ruwisch 2012), was used in the current experiments. The isolated strain (MCP11) was cultivated under sterile aerobic batch condition in yeast extract based medium (20

g/L yeast extract, 0.17 M ammonium sulphate, 0.1 mM $NiCl_2 \bullet 6H_2O$, pH 9.25). After 24 hours incubation at 28°C, the culture was harvested and stored at 4°C prior to use. The optical density (OD_{600}) of the harvested bacterial suspension varied between 1.5 to 2.0, and the urease activity was approximately 10 U/ml (1 U = 1 μmol urea hydrolyzed per min). The $CaCO_3$ precipitation rate, depending on the amount of urease activity introduced, can affect the size of the crystals and in turn the bonding force of the $CaCO_3$ crystal bridges and corresponding strength of the treated soil (Ismail et al. 2002a). In this study, the average $CaCO_3$ precipitation rate was about 10 g/L (solution)/h. The cementation solution consisted of 1 M urea and 1 M $CaCl_2$.

2.3 Sample Preparation

The sample preparation started with packing the dry sand (fine and coarse) into a PVC column of 160 mm in height and 55 mm inner diameter. The final dry density and porosity of the sand samples were about 1.62-1.63 g/cm^3 and 39%, respectively. Various amounts of water were then flushed from top to bottom to provide the desired degree of saturation within the sand matrix. The degree of saturation is the volume of water in the voids, expressed as percentage of the total volume of voids, according the following equation (Eq. 3):

[3] $$\text{Saturation Degree, } S(\%) = \frac{V_{water}}{V_{voids}} \times 100$$

where; V_{water} is the volume of water in the soil matrix and V_{voids} is the volume of voids. Unless otherwise stated, the sample preparation consisted of the following three steps:

1) Alternating injection of equal volumes of bacterial suspension and cementation solution with an inflow rate of about 1 L/hour. The total volume of the introduced solutions was the same as the aforementioned water volume so as to keep a constant degree of saturation. A vacuum pump was connected to the bottom of the PVC column to remove the excess solution.

2) Curing for 12 hours at 25±1^{o}C to allow the bacterial fixation process to complete.

3) Percolation of cementation solution with the same flow rate followed by another curing period of 12 hours at 25±1^{o}C. This step was carried out twice.

It should be noted that, to obtain different mechanical properties of the soil samples, the above-mentioned three steps might be conducted more than once.

The key issue of the above process is to keep a constant degree of saturation throughout the tests by managing the volume of extracted solution to be equal to that of the injected solution. Meanwhile, to avoid solution accumulation at the bottom of the sand column by gravity, the PVC columns were horizontally placed during the curing period. The saturation degrees over the entire 15 cm long sand columns were determined. The local saturation of the columns between 2.5 to 12.5 cm depth was relatively homogenously distributed with a deviation not greater than ±6% saturation. Therefore, the specimens prepared for the mechanical property analyses were taken from about 2 to 13 cm depth of the sand columns.

2.4 Microscopy Investigation

In order to characterize the shapes and locations of the precipitated $CaCO_3$ and to investigate the bonding behaviour between the grain hosts and cement agent, microscopy analysis was conducted on the cemented soil samples, which were taken from the centre of the cemented sand columns. Before conducting the microscopy investigation, all samples were flushed with tap water and dried at 60 °C for 24 hours. The microscopy investigation was carried out using scanning electron microscopy (SEM) PHILIPS XL20 Scanning Electron Microscope, Eindhoven, the Netherlands.

2.5 Unconfined Compressive Strength (UCS) Tests

To quantify the strength imparted into the MICP treated silica sand under different saturation conditions, the unconfined compressive strength (UCS) tests were conducted on cemented specimens of 55 mm in diameter with a selected diameter to height ratio of 1:1.5 to 1:2. The axial load was applied at a constant rate of 1.0 mm/min. Before carrying out the tests, the sand samples were treated with different amounts of MICP under 20%, 40%, 80% and 100% degrees of saturation.

2.6 Triaxial Compression Tests

The triaxial compression test was employed to provide verification for the MICP as a soil stabilization technique. This test is considered to be the most reliable test to measure the shear strength parameters of soils. In this study, a series of single-stage consolidated undrained triaxial tests with pore water pressure measurement were carried out to establish the effective shear strength parameters (i.e., cohesion, c', and friction angle, ϕ') of the bio-cemented sand. Specimens were set under one confining pressure

and sheared till failure. The effective cohesion and friction angle were determined using the Mohr-Coulomb failure envelopes established from three individual samples. All tests were conducted in accordance with the procedures set out by Head (1998). Before carrying out the triaxial tests, the bio-cemented specimens were treated at different degrees of saturation of 30%, 65% and 100%. Each triaxial test started with saturating the sand specimens with tap water so as to achieve a Skempton's *B* value of at least 95%. The specimens were then subjected to confining pressures of 50, 100 and 200 kPa, respectively, and an axial stress was then applied to failure at a strain rate of 1 mm/min. All triaxial tests were performed on specimens of 55 mm in diameter with a selected diameter to height ratio of approximately 1:2. A baseline sample of untreated sand was also tested to allow comparison of the soil improvement properties.

2.7 Permeability Tests

Permeability is a primary factor that controls the behavior of porous materials under saturated conditions and thus dictates the suitability of a specific material for certain applications (Shahin et al. 2011). Porous materials with high permeability can prevent the development of excess pore water pressure during loading. To identify the permeability of cemented sand treated with different amounts of $CaCO_3$ precipitates, more samples were prepared at degrees of saturation of 30%, 65% and 100%, and permeability tests were conducted. The permeability test was also conducted on the untreated samples for the purpose of comparison with the treated samples. The untreated fine sand has a hydraulic conductivity of 9.2×10^{-5} m/s, whereas it is 44.7×10^{-5} m/s for the untreated coarse sand.

Laboratory determination of the permeability of the untreated and bio-cemented sand was conducted using constant head permeability test with a rigid side wall device in accordance with the Australian Standards AS 1289 (2007). All specimens were saturated prior to the permeability test by flushing through 2 L tap water under 15 kPa back pressure (hydraulic head of about 150 cm) to remove most of the remained pore air.

In order to compare the permeability of the MICP improved soil with conventional soil improvement using chemical additives, a series of mixtures of fine sand with various proportions of Portland cement were prepared and tested for their strength and permeability. The details of the Portland cement samples are listed in Table 1. The mixtures were poured into PVC columns with the same dimension of that used for bio-cementation, and a strong vibration was applied to avoid any air bubbles that might remain in the mixture. The prepared mixtures were then cured at the room temperature (20±1 ^{o}C) for 7 days prior to the UCS and permeability measurements.

2.8 Durability Tests

2.8.1 Freeze-Thaw Durability

To test the resistance of MICP cemented samples to freeze-thaw (FT) cycling, a series of fine sand samples (110 mm in height and 55 mm in diameter) treated by MICP and Portland cement, as described previously, was subjected to 10 cycles of FT actions. Each cycle test involves subjecting the samples to a 12-hour freeze at –14 ^{o}C followed by a 12-hour thaw under ambient conditions (20±1 ^{o}C). All samples were immersed in water throughout the cycling FT testing.

2.8.2 Acid Rain Durability

Artificial acid rain was made according to Haneef et al. (1992) and the final pH of acid rain was adjusted to 3.5 by adding additional H_2SO_4. The artificial acid rain was injected from the top of the cemented fine sand columns (180 mm in height and 55 mm in diameter) with a flow rate of approximately 3 mL/min. The weight of the sand column was measured periodically, after it was washed by DI water and dried at 105 ^oC for 12 hours. All samples were cut in half prior to the shear strength test and the strength of the top and bottom parts of the sand samples (eroded and un-eroded) was recorded.

3 Presentation of Results

3.1 Effect of Degree of Saturation on UCS Results of MICP Cemented Coarse Sand

Figures 2 and 3 show the results of the UCS tests carried out on the coarse sand treated with different amounts of MICP under various saturation degrees of 20%, 40%, 80% and 100%. It can be seen that both unconfined compressive strength (q_{ucs}) and stiffness (or elastic modulus, E) increase with the increase of $CaCO_3$ content for all treated samples. Both q_{ucs} and E follow exponential relationships with the content of $CaCO_3$, which are in line with previous results reported by van Paassen et al. (2010). It can also be seen that for the same amount of $CaCO_3$ precipitation, both q_{ucs} and E increase with the reduction in the degree of saturation. Saturation degree higher than 80% was found to have little impact on q_{ucs} and E of MICP treated coarse sands.

213 It is worthwhile mentioning that the failure mechanism of the cemented sand was
214 different from the strong to the weak samples. In the weak samples, the broken cores
215 completely lost strength at the grain scale around the failure plane, or through the entire
216 sample when the failure planes were not clear. This was consistent with previous
217 observation by van Paassen et al. (2009). In the strong samples, however, tensile cracks
218 appeared vertically from top to bottom along the sample and the failure planes can be
219 distinguished clearly, which was also similar to the previous observation by van
220 Paassen et al. (2009).

221 It is of interest to examine the location of MICP treated coarse silica sand in the
222 spectrum of other geomaterials in terms of the relationship between E and q_{ucs}, as shown
223 in Figure 4. The change in the rigidity of the MICP treated silica sand is also shown in
224 Figure 5 (rigidity = $E/q_{ucs} = 1/\varepsilon_f$, where ε_f is the axial strain at failure). It can be seen that
225 the rigidity increases (in an exponential law fashion) with increase of $CaCO_3$ content,
226 but was independent of the degree of saturation. It can also be seen that at similar
227 amount of $CaCO_3$, the rigidity of the samples cemented at lower degree of saturation
228 was higher than that of the samples treated with higher degree of saturation. Similar to
229 the effect of saturation on q_{ucs}, a degree of saturation higher than 80% had marginal
230 impact on the rigidity of MICP cemented sand for certain amount of $CaCO_3$ content.

231 **3.2 Microscopy Images of MICP Cemented Sand at 20% and 100% Saturation**

232 In this part, an attempt is made to investigate the reason for increasing strength and
233 stiffness of the MICP treated sand at lower degree of saturation. It is believed that the
234 micro-features of precipitated crystals around the sand grains and the creation of hinges
235 can be responsible for the different mechanical responses of MICP treated porous

materials obtained at different saturation conditions (Paraskeva et al. 2000). In order to investigate this matter, the micro-structure of the treated sands was investigated through the microscopy images shown in Figures 6 and 7 for soil treated at degrees of saturation of 100% and 20%, respectively.

It can be seen from the images shown in Figure 6 that the $CaCO_3$ crystals produced at 100% saturation take rhombohedron form in which the agglomerated rhombohedral crystals precipitate not only in the inter-particle contact points but also on the grain surface, or suspend in the pore spaces, leading to insufficient connections between the sand grains. For the sand treated at 20% saturation (Figure 7), a strong coating effect of the MICP process is predominant. This coating effect is likely attributed to the homogeneously adsorbed solution on the sand grains surface due to the surface tension force, which allows the MICP solution to access the full surface of the grains. One important feature that can be derived from Figure 7 is that the gaps between the host grains are almost completely filled with crystals, which is likely due to the fact that the retained MICP solution located between the grains takes a menisci form, where the crystals are produced and precipitated out of the aqueous solution to fill the gaps. This feature may affect the adhesion mechanism amongst the host grains and, consequently, the mechanical behavior of the entire soil matrix.

It should be noted that both samples treated at 100% saturation (Figure 6) and 20% saturation (Figure 7) demonstrate similar q_{ucs} of 1 MPa and 1.14 MPa，respectively, but they differ in the $CaCO_3$ content. It is apparent that the development of the $CaCO_3$ at the contact boundary is vastly different in both cases, and in comparison it can be identified that an excess precipitation of the $CaCO_3$ at the sand grain boundary exists for

the case of 100% saturation condition. As a result, the sample treated at 20% saturation contained fewer $CaCO_3$ crystals less than half of that precipitated at 100% saturation (i.e. 0.143 g/g sand). This indicates that the mechanical strength of the MICP treated samples is due to the effectiveness of $CaCO_3$ formation that precipitated in the inter-particles contact points, rather than the total amount of the $CaCO_3$ crystals formed.

The schematic diagram shown in Figure 8 can provide further explanation of the previous observation. For partially saturated condition, the air occupies the center of the pores and the total surface of the grains is covered with adsorbed solution, which is predominantly concentrated at the inter-particles connection points (corner) forming menisci shape (Tuller et al. 1999). Therefore, the crystal precipitation has mainly occurred at the contact points of the grains (Figure 8), which contributes to the strength improvement. In the case of full saturation, as the MICP solution occupies the entire pore space, the crystals are free to precipitate without being restricted to the size and location, resulting in the agglomerated crystals to be formed on both the host grain surface and grain gaps. From the above discussion, it can be stated that the crystals formation varies in size and location according to the distribution of pore solution, which is influenced by the saturation conditions.

3.3 Mathematical Model of Total Volume of Effective Hinges

In Sections 3.2 and 3.3, it was experimentally shown (through microscopy images and results of UCS tests) that the degree of saturation at which a sand soil is treated by MICP has a significant impact on the resulting strength and stiffness. Also the particle size of the constituent soil affects the cementation process, because it has a significant impact on the retained pore water in terms of the content, shapes and distribution under

various saturation conditions, consecutively on the cementation process. In this section, a mathematical model is developed in order to measure the impact of the saturation degree and particle size on the effective "hinge" formation within a soil matrix treated with MICP.

In order to develop the mathematical model, a soil matrix with uniform spherical particles is assumed. All spherical particles are packed in a tetrahedral packing form having the closest packing order with a void ratio of 0.34. The total volume of the sand matrix (V) and void volume (V_{void}) can be approximately calculated as follows:

[4] $$V = N \times (4/3) \times \pi \times R^3 / (1 - 0.34)$$

[5] $$V_{void} = 0.34 \times V$$

where; N is the number of particle spheres and R is the radius of the sphere (see Figure 9).

In the assumed tetrahedral packing, each particle has 12 contact points with the surrounding particles and there are 6 full water lenses in each unit volume of $5.66R^3$ (Lu and Likos 2004). The total number of water lenses (N_{lens}) in the sand matrix therefore can be calculated as follows:

[6] $$N_{lens} = 6 \times V / (5.66 \times R^3)$$

The crystals are assumed to be homogeneously precipitated on the surface of spheres, where the water lenses are attached, and the crystal "hinges" formed in point-to-point

301 contacts contribute to the bonding force. In general, it is reasonable to make the
302 hypothesis that the bigger volume of "hinges" causes stronger bonding force. From
303 Figure 9b, the total volume of effective hinges ($V_{T\text{-}hinges}$) in the soil matrix can be
304 calculated as follows:

305 [7] $$V_{T-hinges} = N_{lens} \times V_{hinge} = N_{lens} \times (2\pi \times r^2 h' - 2\pi / 3 \times h'^2 (3r - h'))$$

306 where; V_{hinge} presents the volume of each hinge, and h' & r are as illustrated in Figure
307 9b, which can be obtained based on the following geometric calculations:

308 [8] $$h' = R - \sqrt{R^2 - r^2}$$

309 [9] $$r = \sqrt{(R+h)^2 - R^2}$$

310 In Eqns. 8 and 9, h is the thickness of crystals on each sphere and can be estimated as
311 follows:

312 [10] $$h = V_{crystals} / (2 \times S_{surface})$$

313 where; $V_{crystals}$ is the volume of $CaCO_3$ crystals precipitated on each sphere and $S_{surface}$ is
314 the contact surface between the water lens and the sphere (see Figure 9a and b). Both
315 $V_{crystals}$ and $S_{surface}$ can be calculated according to the following expressions:

316 [11] $$V_{crystals} = C_{crystals} \acute{} V / r_{crystal} / N_{lens}$$

317 [12] $$S_{surface} = 2\pi \times (R+h)^2 \times (R - (R+h) \times \cos(\theta))$$

where; $C_{crystals}$ is the $CaCO_3$ crystals content (g/cm^3) and $\rho_{crystals}$ is density of $CaCO_3$ crystals (i.e. 2.71 g/cm^3).

The degree of saturation of the soil matrix can also be obtained as follows:

[13] $$S_{saturation}\% = V_{water} / V_{void} = N_{lens} \times V_{lens} / V_{void}$$

where; V_{lens} is the volume of each water lens, which can be calculated in accordance with Dallavalle (1943), as follows:

[14] $$V_{lens} = 2\pi \times R^3 \times (1/\cos(\theta) - 1)^2 \times [1 - (\pi/2 - \theta) \times \tan(\theta)]$$

The developed mathematical model (i.e. Eqns. 7 and 14) was used to illustrate the dependency of the total volume of effective "hinges" formed in the same volume of sand matrixes on the degree of saturation and particle size (see Figure 10). The number of spherical particles, *N*, is inversely proportional to the particle size (*R*), providing the same total matrix volume. This means that if the coarse sand particle has a radius *R* while the fine sand particle has a radius *R/2*, the number of particles of the fine sand will be eight times that of the coarse sand. Consequently, the total number of water lenses (N_{lens}) in the fine sand matrix will be eight times that of the coarse sand.

The model predictions shown in Figure 10 indicate that a greater volume of effective hinges is formed in the fine sand compared to the coarse sand having similar amount of $CaCO_3$ precipitation, indicating that the strength is improved with the decrease in particle size. This model also derives that a lower degree of saturation leads to a greater number of effective hinges at the same $CaCO_3$ content and consequently an improved

mechanical behavior (i.e. UCS). The model predictions are supported by the previous experimental UCS tests and microscopy images of the coarse sand.

To further investigate the real effect of particle size and degree of saturation on the shear strength parameters of treated sand (i.e., cohesion, *c'*, and friction angle, ϕ'), which are more relevant to most geotechnical engineering applications, the results of the undrained triaxial tests are presented below.

3.4 Mechanical Behavior of Stabilized Sand in Triaxial Tests

The effective shear strength parameters (i.e. cohesion, *c'*, and friction angle, ϕ') of the silica sand treated with different amounts of $CaCO_3$ were determined from the Mohr-Coulomb envelopes. These were developed from the peak shear stress values obtained from the triaxial tests. Results are shown in Figures 11 and 12, for coarse and fine sands, respectively.

Coarse Sand

Figure 11 shows that both the cohesion, *c'*, and friction angle, ϕ', increase with the increase of the $CaCO_3$ content at all degrees of saturation. At a fixed amount of $CaCO_3$ a lower saturation degree increased the *c'* and ϕ' values compared to those at higher saturation degrees. Under lower saturation degree condition, the precipitated crystals contributed more to improving cohesion than to improving friction angle. At higher saturation degrees of 65% and 100%, the impact on improving the friction angle was even less. As mentioned earlier, the effect of degree of saturation on improving the shear strength behavior of soil and thus the shear strength parameters is attributed to

restricting the crystal formation mainly to the connection points. The well-placed crystals are efficient in increasing the inter-particle connection, thereby, enhancing the soil cohesion and friction angle. The increase in both cohesion and friction angle at higher $CaCO_3$ content that has occurred regardless of the saturation degree is likely due to the fact that precipitated crystals start filling the pore spaces. One important feature that can be derived from Figure 11 is that at low $CaCO_3$ content the friction angle had only marginally increased under all saturation conditions, which was probably due to the slight increase in the dry density. The optimum condition for c' and ϕ' has occurred at the saturation condition of 30%.

Fine Sand

Figure 12 shows that the overall correlation between the shear strength parameters and the $CaCO_3$ content at different saturation degrees is similar to that of the coarse sand. By comparing the results of the two sands used, it can be concluded that under the same saturation condition, the coarse sand demonstrates higher friction angle than the fine sand at similar $CaCO_3$ content. The fine sand with similar $CaCO_3$ content showed significantly higher values of cohesion compared to the coarse sand. This can be explained as follows. Smaller particles have two effects including: (a) providing more inter-particle contact points for microbially induced $CaCO_3$ to precipitate; and (b) reducing the stress acting per particle contact. MICP acts most efficiently at a particle contact just as cementation begins, and continued expansion of cementation around a particle contact has decreased effect. Therefore, reallocating the $CaCO_3$ crystals to two contact locations instead of one would be more effective. At the same time, the contact stress decreases as a function of the particle radius squared. Therefore, smaller particles

provide two compounding benefits: (1) more efficient MICP; and (2) lower particle contact stresses.

3.5 Effect of MICP Treated Sand on Permeability

Figure 13 shows the results of permeability tests conducted in the current study. It can be seen that a reduction in permeability was encountered for all bio-cemented sand samples. In contrast to the phenomenon reported by Whiffin et al. (2007), the permeability decreased with an increase in $CaCO_3$ content for both fine and coarse sands, irrespective of the saturation degree. Results suggest that it is preferable to conduct the MICP process under lower saturation conditions, as it enabled improved mechanical behavior at the same time as maintaining relatively high residual permeability.

Figure 14 shows the results of comparison between sand samples treated with Portland cement and bio-cement. It can be seen that the bio-cement samples have higher strength in the range of lower cement agents content (< 0.1 g/g sand) compared to the Portland cement samples after 7 days of curing. However, this comparison would differ depending on the applied curing time of the Portland cement samples. The permeability of the biocementation samples is significantly higher than that of the Portland cement samples. As an example, a mixture with 7% (0.07 g/g sand) Portland cement dramatically decreased permeability by 98%. Cement content higher than 9.6% (0.096 g/g sand) produced a poor drainage material with permeability less than 1×10^{-6} m/s. The significant loss of permeability in the Portland cement samples is due to the occupation of the pore space by the water insoluble hydrates formed from the cement hydration reaction with the pore water. In contrast, the loss of permeability in bio-

405 cement samples is caused by the pore spaces becoming occupied by the calcite crystals,
406 which only causes a smaller volume change compared to the hydrates.

407 From the previous results, it can be concluded that apart from the significant increase in
408 soil strength and stiffness, one advantage of biocementation is attributed to the relative
409 ability to retain soil permeability after treatment, compared to the traditional chemical
410 treatment by Portland cement.

411 **3.6 Effect of MICP Treatment on Sand Freeze-Thaw Durability**

412 Destruction of porous materials caused by freezing and thawing has been of great
413 concern to engineers for more than 200 years (Johnson 1952). The phase change of
414 water adsorbed in the soil pores is the most significant cause of deterioration of exposed
415 porous materials. Porous solids with high porosity or permeability usually have a good
416 service record after free-thaw (FT) action (Litvan 1980). Indicated by the previous
417 permeability results, the sand samples treated with MICP have a high residual
418 permeability, which may favor the samples to endure the cycled FT action.

419 By comparing the UCS of MICP tested samples before and after FT cycling, less than
420 10% decrease in strength occurred irrespective of the treatment conditions (Figure 15).
421 The severity of the mechanical damage is proportional to the water content of the
422 porous solid (Litvan 1980); however, the high porosity and permeability allow more
423 rapid water mass transfer in the sand matrix, which can increase the FT resistance. For
424 MICP samples, the crystals formed at the contact points can maintain the connection of
425 pores without restricting the pore water mobility, which is also proved by the previous

permeability tests. For the Portland cement samples, the FT cycles caused serious damage, as expected, with about 40% decrease in strength.

3.6.1 Acid Rain Erosion Durability

Acid rain is detrimental to many construction materials, particularly those made from limestone or sand stone with high $CaCO_3$ content. The chemical reaction between the calcium carbonate and sulfuric acid (the primary acid component of acid rain) causes the dissolution of $CaCO_3$, resulting in destruction of such materials. In the MICP treated sand, the strength of sand matrix is the result of the sand particles bonded by the bridging $CaCO_3$ crystals. Therefore, the $CaCO_3$ crystals eroded by the acid rain will result in destruction of the connections between the sand particles, leading to severe damaging in mechanical properties.

In order to test erosion and residual strength of the MICP treated sand samples after exposure to the acid rain, in time mass detection of the sand matrix and UCS tests were carried out and the results are presented in Figure 16. It can be seen that, as expected, the artificial acid rain (pH=3.5) continuously eroded the biocement samples, resulting in a loss of weight. The pH of the effluent stayed around 7.5, which indicated that the protons (H^+) in the acid rain were consumed by reacting with $CaCO_3$, similar to the acid rain erosion of limestone and marble. After flushing 12 L of acid rain through the sand column, corresponding to 5 years of rainfall (1000 mm/year), the UCS results of the eroded samples reflected that no obvious damage occurred at the bottom part of the sand column (9-18 cm). However, the strength of the top part of the sand column was decreased by about 40%, as shown in Figure 16. As the effect of the acid rain is chronic

and long-term acidification results from years of acidic rainfall, a long-term simulation experiment (decades) is worthwhile to carry out in the future.

4 Discussion

This study verified that the bio-cementation technology applied to partially saturated soils lead to improved mechanical behavior of MICP treated soil matrix in terms of cohesion, friction angle and UCS, with fewer calcite crystals compared to MICP at fully saturated condition. In other words, to produce similar soil strength, partially saturated soils require fewer crystals, enabling bio-cemented soils to be produced more economically due to lower requirement for the urease enzyme, urea and $CaCl_2$. To this end, the technique can be applied to many geotechnical-engineering applications in both fully and partially saturated conditions. In wet fully saturated condition, MICP solution is introduced into the soil by saturated flow (van Paassen et al. 2010; Whiffin et al. 2007). In dry or partially saturated condition, MICP solution can be introduced by surface percolation and the excess of MICP solution moves deeper into the soil pores, which allows the retained MICP solution to accumulate at the connection points as a meniscus shape (Cheng and Cord-Ruwisch 2012). The restricted distribution of MICP solution enables the crystals formed at the particular position, which contributes the most to strength development. However, an obvious main challenge for MICP treatment under unsaturated conditions is achieving homogenous distribution of $CaCO_3$ and strength, which will be investigated in subsequent phase of this work.

A principal engineering problem produced by current available soil improvement methods is the tendency of significantly decreasing permeability of treated soils. For

example, the reduction in permeability due to grouting ranges between 2 and 3 orders of magnitude (Karol 2003). Consequently, the reduction in permeability disturbs natural groundwater flow paths, permits the increase of pore water pressure in the soil, thus increasing the risk of failure in both earth and foundation structures. The ability of MICP to retain high permeability conditions is a clear advantage compared to the alternative of using Portland cement. A reduction in the cost of construction and installation of drainage systems would be apparent, as fewer systems would need to be integrated than those typically utilizing traditional cementing agents. Another advantage of MICP and its retention of *in-situ* permeability during bio-cementation application is that it will permit additional applications of treatment allowing engineers to control the final strength.

Engineering examples of the utilization of MICP and the associated benefits of permeability retention would be in the reinforcement of transport subgrades and embankments. During subgrade construction it is important to provide adequate drainage at all times to prevent water from standing on the subgrade. Therefore, soil stabilization by MICP technique with the capability of high permeability retention would eliminate the need for additional drainage systems. Due to the minimal interference with soil material hydrology, embankments strengthened with MICP will have the potential to allow immediate dissipation of excess pore water pressures caused by operational surcharge loads.

Geotechnical engineering structures exposed to dynamic loads associated with earthquakes under saturated conditions can be subject to significant structural damage. In this case, the soil loses most of its static strength and significant deformations occur.

When such deformations are large, soils liquefy (Cornforth 2005). The soil types most susceptible to liquefaction are loose granular sands that have no cementation between the soil grains. Given the improvements in the undrained shear strength of sands trialed in this study, MICP can be used as a viable solution to improve the properties of un-cemented granular soils by creating cemented zones that will be no longer liquefiable.

5 Conclusions

This paper has investigated the influence of degree of saturation and soil particle size on the mechanical response of calcite bio-cemented silica sand. Samples examined under SEM indicated different patterns of calcite precipitation for each degree of saturation, with fully saturated condition forming agglomerated rhombohedral crystals scattered on the sand grain surface. The lower saturated conditions formed strong calcite coating on the host grains and bridging between sand grains. A mathematical model has been also developed, which measures the impact of the degree of saturation and particle size on the effectiveness of $CaCO_3$ precipitates in MICP treated soils.

Findings of this study confirmed that higher strengths were obtained at lower saturation degrees, challenging most studies on MICP so far, in which biocementation was performed under fully saturated condition. This important finding indicates that optimum performance of this stabilization process can be achieved with lower costs, making it economically viable while reducing the need for water and chemicals, hence, becoming more environmentally sustainable than formerly believed.

The results from the durability tests have shown that MICP produced cemented samples with highly durable resistance to freeze-thaw erosion, and resistless to the acid rain

erosion. Both the permeability and shear strength of bio-cemented soils displayed results that would support the MICP as a promising soil improvement technique. MICP has been approved to be a viable alternative for engineering soil improvement applications such as soil embankments, liquefiable sand deposits and subgrade reinforcement.

The results obtained from the UCS and triaxial tests have shown that, despite having the same amount of calcite crystals, the engineering response of treated sand varies significantly, mainly because of the different location of the calcite deposited. The calcite crystals formed under lower degree of saturation showed that more crystals are formed in the contact points, which contributed to the strength of the cemented samples.

6 Acknowledgement

The authors would like to acknowledge Deltares (the Netherlands) and University of Murdoch (Australia) for the financial support given to this project. The authors would also like to thank Atticus Dekuyer for providing assistance in the triaxial measurements.

7 References

Australian Standards AS 1289, 2007. Method of testing soils for engineering purposes.

Al-Thawadi, S., and Cord-Ruwisch, R. 2012. Calcium carbonate crystals formation by ureolytic bacteria isolated from Australian soil and sludge. Journal of Advance Science and Engineering Research, 2 (1): 13-26.

Barla, M., Barla, G., Lo Presti, D.C.F., Pallara, O., and Vandenbussche, N. 1999. Stiffness of soft rocks from laboratory tests. Proceedings of the IS Torino '99, 2nd International Symposium on Pre-failure deformation characteristics of

geomaterials. Torino, 26-29 September 1999.

Burbank, M.B., Weaver, T.J., Green, T.L., Williams, B.C., and Crawford, R.L. 2011. Precipitation of calcite by indigenous microorganisms to strengthen liquefiable soils. Geomicrobiology Journal, 28(4): 301-312.

Cheng, L., and Cord-Ruwisch, R. 2012. *In-situ* soil cementation with ureolytic bacteria by surface percolation. Ecological Engineering, 42: 64-72.

Cornforth, D.H. 2005. Landslides in practice: investigation, analysis, and remedial/preventative options in soils. John Wiley & Sons, Inc.

Dallavalle, J.M. 1943. Micrometrics. Pitman, London.

DeJong, J. T., Fritzges, M. B., and Nusslein, K., 2006. Microbially Induced Cementation to Control Sand Response to Undrained Shear. Journal of Geotechnical and Geoenvironmental Engineering, 132 (11): 1381- 1392.

DeJong, J. T., Mortensen, B. M., Martinez, B. C., and Nelson, D. C. 2010. Biomediated soil improvement. Ecological Engineering, 36 (2): 197-210.

Haneef, S.J., Dickinson, C., Johnson, J.B., Thompson, G. E., and Wood, G.C. 1992. Simulation of the degradation of coupled stones by artificial rain. Studies in Conservation, 37(2): 105-112.

Head, K.J.H. 1998. Manual of Soil Laboratory Testing. John Wiley and Sons, Chichester, England.

Ismail, M.A., Joer, H.A., Randolph, M.F., and Meritt, A. 2002a. Cementation of porous materials using calcite. Géotechnique, 52(5): 313-324.

Ismail, M.A., Joer, H.A., Sim, W. H., and Randolph, M.F. 2002b. Effect of cement type on shear behavior of cemented calcareous soil. Journal of Geotechnical and Geoenvironmental Engineering, 128(6): 520-529.

Johnson, A.W. 1952. Frost action in roads and airfield-a review of the literature. Special Report No. 1, Highway research board, Washington, D.C.

563 Karol, R. H. 2003. Chemical Grouting and Soil Stabilization. New York, Marcel
564 Dekker.

565 Litvan, G.G. 1980. Freeze-thaw durability of porous building materials, durability of
566 building materials and components. ASTM STP 691. P. J. Sereda and G. G. Litvan,
567 Eds, American Society for testing and materials, 1980, pp. 455-463.

568 Lu, N., and Likos, W.J. 2004. Unsaturated soil mechanics. John Wiley & Sons, Inc.
569 New Jersey.

570 Mitchell, A., and Ferris, F. 2006. The influence of bacillus pasteurii on the nucleation
571 and growth of calcium carbonate. Geomicrobiology Journal, 23(3-4): 213-226.

572 Paraskeva, C.A., Charalambous, P.C., Stokka, L.E., Klepetsanis, P.G., Koutsoukos,
573 P.G., Read, P., Ostvold, T., and Payatakes, A.C. 2000. Sandbed consolidation with
574 mineral precipitation. Journal of Colloid and Interface Science, 232: 326-339.
575 doi:10.1006/jcis.2000.7161

576 Shahin, M.A., Mardesic, T., and Nikraz, H.R. 2011. Geotechnical characteristics of
577 bauxite residue sand mixed with crumbed rubber from recycled car tires. Journal of
578 GeoEngineering, 6(1): 63-72.

579 Tuller, M., Or, D., and Dudley, L.M. 1999. Adsorption and capillary condensation in
580 porous media: liquid retention and interfacial configurations in angular pores. Water
581 Resource Research, 35 (7): 1949–1964.

582 van Paassen, L.A., Ghose, R., Van der Linden, T.J.M., Van der Star, W.R.L., and Van
583 Loosdrecht, M.C.M. 2010. Quantifying biomediated ground improvement by ureolysis:
584 large-scale biogrout experiment. Journal of Geotechnical and Geoenvironmental Engineering,
585 136(12): 1721-1728.

586 van Paassen, L.A., van Lossdrecht M.C.M., Pieron, M., Mulder,A., Ngan-Tillardm
587 D.J.M., and van der Linden, T.J.M. 2009. Strength and deformation of biologically
588 cemented sandstone. proceedings of the ISRM Regional conference EUROCK 2009-
589 Rock engineering in difficult ground conditions- Soft rocks and karst, 29-31 October
590 2009, Dubrovnik, Croatia, pp. 405-410.

591 Warren, A.A., Maurice, P.A., Parmar, N., and Ferris, F.G. 2001. Mirobially mediated
592 calcium carbonate precipitation: Implications for interpreting calcite precipitation and
593 for solid-phase capture of inorganic contaminants. Geomicrobiology journal, 18(1): 93-
594 115.

595 Whiffin, V.S., van Paassen, L.A., and Harkes, M.P. 2007. Microbial carbonate
596 precipitation as a soil improvement technique. Geomicrobiology Journal, 24(5): 417-
597 423.

598 **Table 1.** Mix proportions of Portland cement samples.

Mix ID	Cement (g)	Sand (g)	Water (mL)	Density (g/cm^3)
1	40	580	124	1.93±0.01
2	56			
3	72			
4	84			

599

Figure Captions:

Figure 1. Grain size distribution curves for the sand used.

Figure 2. Variation of UCS with $CaCO_3$ content and different saturation conditions for coarse sand.

Figure 3. Variation of stiffness with $CaCO_3$ content and different saturation conditions for coarse sand**.**

Figure 4. Relationship between elastic modulus (E) and q_{ucs} of the MICP treated silica sand compared with other geomaterials.

Figure 5. Relationship between rigidity and CaCO3 content for silica sand treated with MICP under different water saturation degree conditions.

Figure 6. Formation of $CaCO_3$ crystals for samples treated at 100% saturation (note: $CaCO_3$ content = 0.143 g/g sand, UCS = 1 MPa).

Figure 7. Formation of $CaCO_3$ crystals for samples treated at 20% saturation (note: $CaCO_3$ content = 0.057 g/g sand, UCS =1.14 MPa).

Figure 8. Conceptual illustration of pore cementation solution distributed in the sand matrix under different saturation conditions.

Figure 9. Schematic diagram of two-dimensional meniscus between spherical particles: (a) water lens between two particles; and (b) simple two-dimensional geometrical illustration of hinge formation between two particles.

Figure 10. Results of mathematical model showing the correlation of the $CaCO_3$ content and volume of effective hinges within the soil matrix for coarse and fine sands (R_{CS} and R_{FS} represent the radii of the coarse and fine particles, N represents the number of particle spheres.).

Figure 11. Effect of saturation conditions on shear strength parameters of coarse silica sand having different amount of $CaCO_3$**.**

Figure 12. Effect of saturation conditions on shear strength parameters of fine silica sand having different amount of $CaCO_3$**.**

Figure 13. Permeability of cemented sand columns treated at different saturation conditions for: (a) coarse sand; and (b) fine sand.

Figure 14. UCS and permeability of sand samples cemented with bio-cement $CaCO_3$ (100% saturation) and Portland cement.

Figure 15. UCS of cemented fine sand samples before and after 10 cycles of Freeze-Thaw (FT) action (one cycle per day). (Note: $CaCO_3$ content was about 0.06-0.065 g/g sand and Portland cement content was 0.096 g/g sand).

Figure 16. UCS and loss of weight of MICP cemented fine sand samples during the acid rain erosion experiments (Note: sand columns were treated under fully saturated condition with $CaCO_3$ content of about 0.1-0.105 g/g sand).

Fig. 1

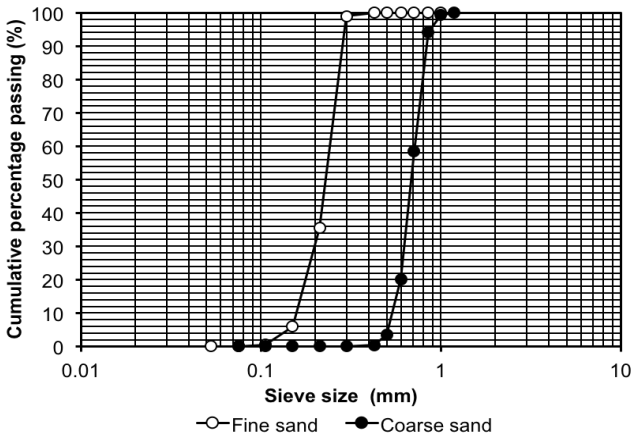
Cumulative percentage passing (%)
100
90
80
70
60
50
40
30
20
10
0
0.01
0.1
1
10
Sieve size (mm)
Fine sand
Coarse sand

Fig. 2

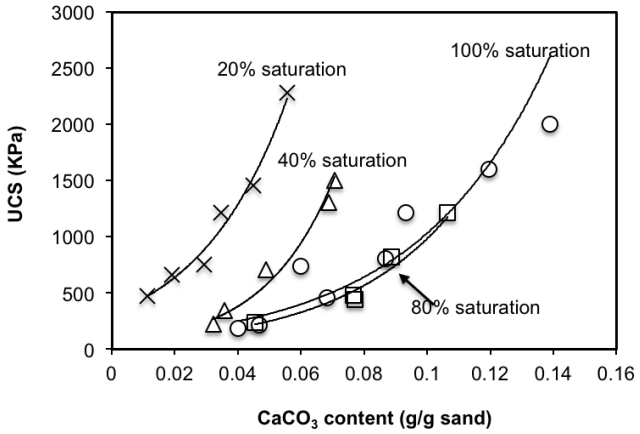
3000
2500
2000
1500
1000
500
0
UCS (KPa)
0
0.02
0.04
0.06
0.08
0.1
0.12
0.14
0.16
CaCO3 content (g/g sand)
20% saturation
40% saturation
80% saturation
100% saturation

Fig. 3

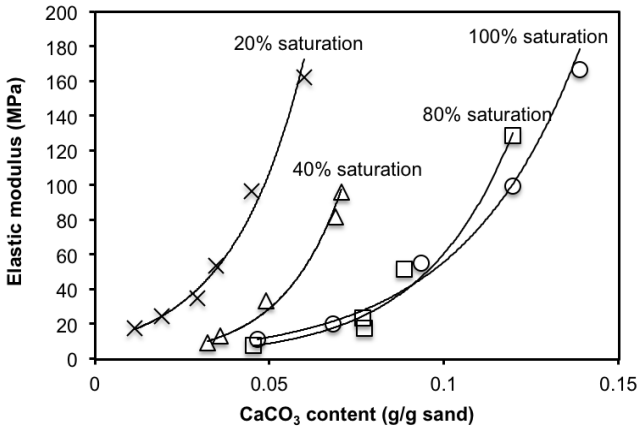
200
180
160
140
120
100
80
60
40
20
0
Elastic modulus (MPa)
20% saturation
100% saturation
80% saturation
40% saturation
0
0.05
0.1
0.15
CaCO3 content (g/g sand)

Fig. 4

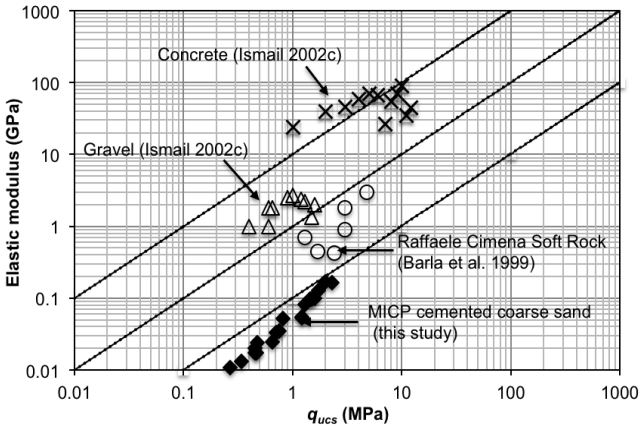
1000
100
10
1
0.1
0.01
Elastic modulus (GPa)
Concrete (Ismail 2002c)
Gravel (Ismail 2002c)
Raffaele Cimena Soft Rock
(Barla et al. 1999)
MICP cemented coarse sand
(this study)
0.01
0.1
1
10
100
1000
q_{ucs} (MPa)

Fig. 5

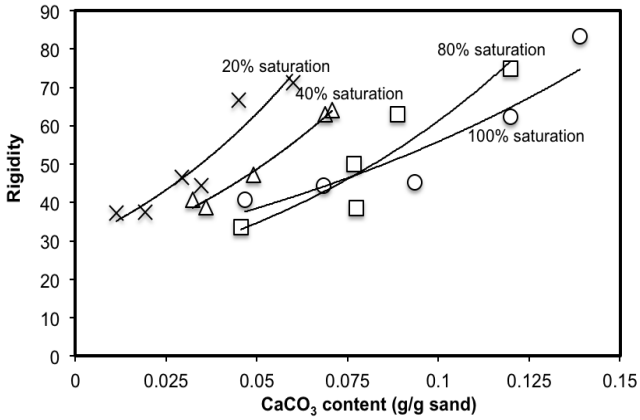
Rigidity
90
80
70
60
50
40
30
20
10
0
0
0.025
0.05
0.075
0.1
0.125
0.15
CaCO3 content (g/g sand)
20% saturation
40% saturation
80% saturation
100% saturation

Fig. 6

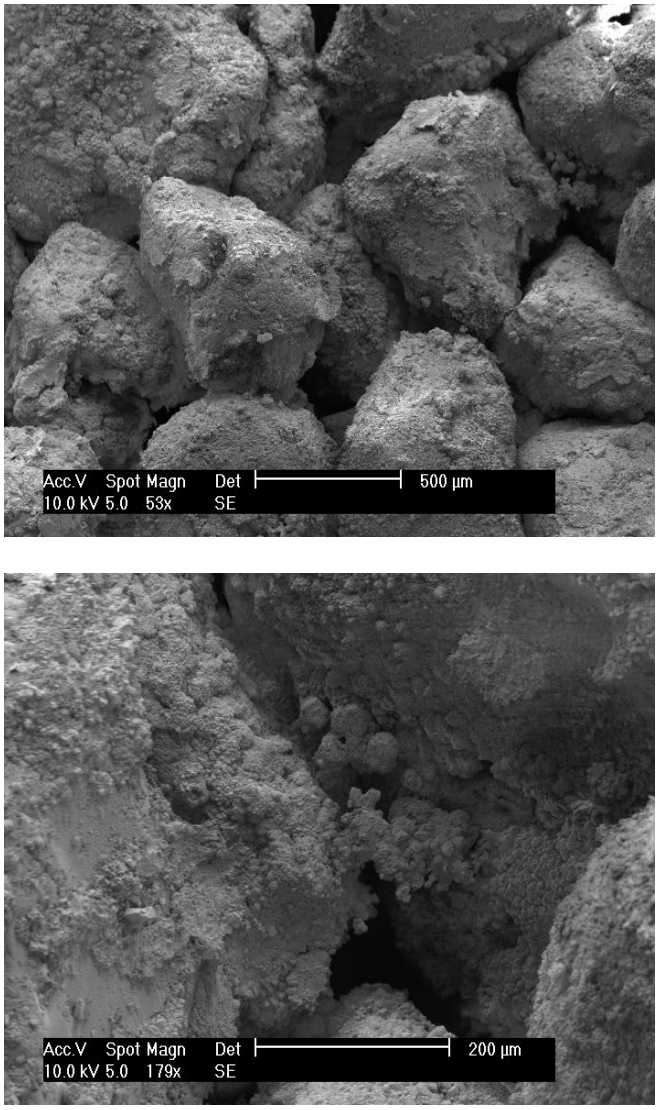
Acc.V Spot Magn Det 500 µm
10.0 kV 5.0 53x SE
Acc.V Spot Magn Det 200 µm
10.0 kV 5.0 179x SE

Fig. 7

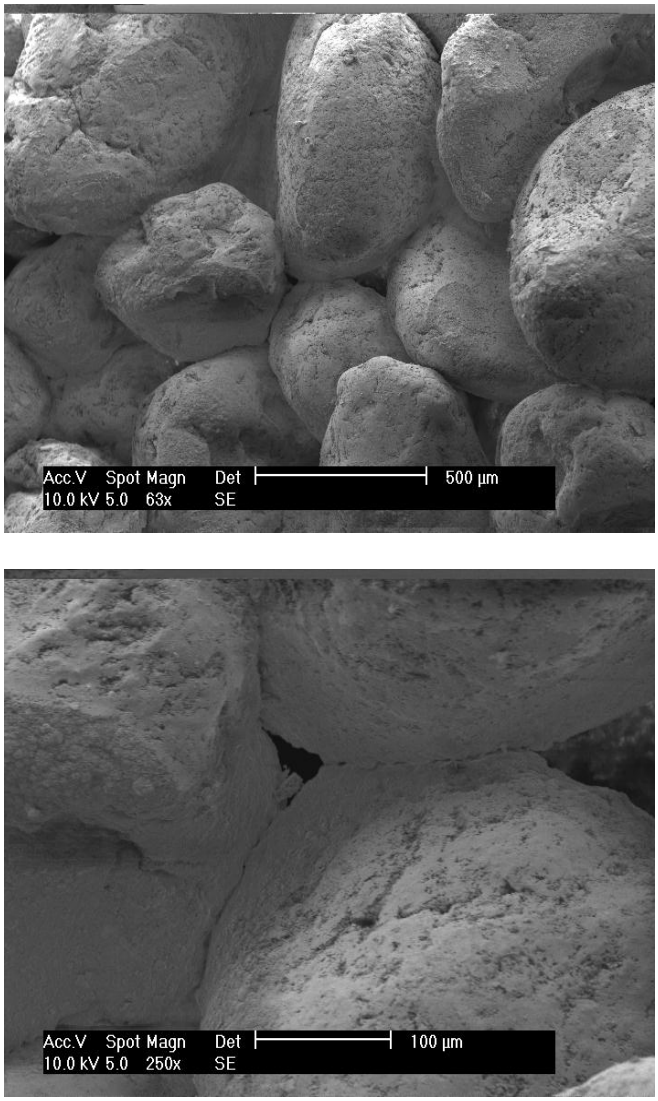
Acc.V Spot Magn Det 500 µm
10.0 kV 5.0 63x SE
Acc.V Spot Magn Det 100 µm
10.0 kV 5.0 250x SE

Fig. 8

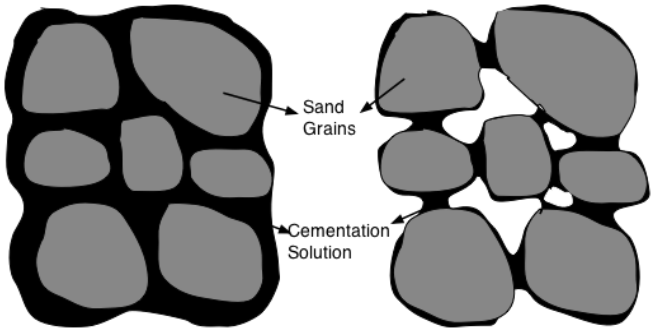

100% saturation 20% saturation

Fig. 9

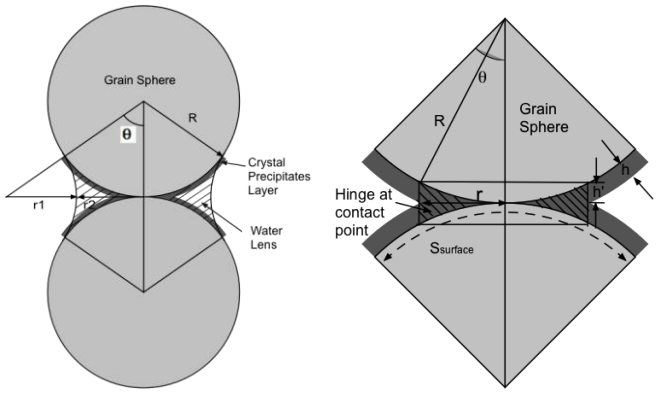
Grain Sphere
R
θ
Crystal
Precipitates
Layer
r1
r2
Water
Lens
θ
R
Grain
Sphere
h
h'
r
Hinge at
contact
point
Ssurface

(a) (b)

Fig. 10

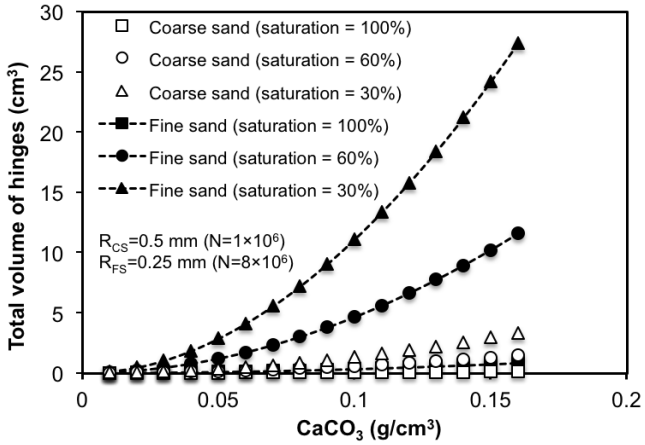
Coarse sand (saturation = 100%)
Coarse sand (saturation = 60%)
Coarse sand (saturation = 30%)
Fine sand (saturation = 100%)
Fine sand (saturation = 60%)
Fine sand (saturation = 30%)
R_CS=0.5 mm (N=1×10^6)
R_FS=0.25 mm (N=8×10^6)
Total volume of hinges (cm³)
CaCO3 (g/cm³)
0
5
10
15
20
25
30
0
0.05
0.1
0.15
0.2

Fig. 11

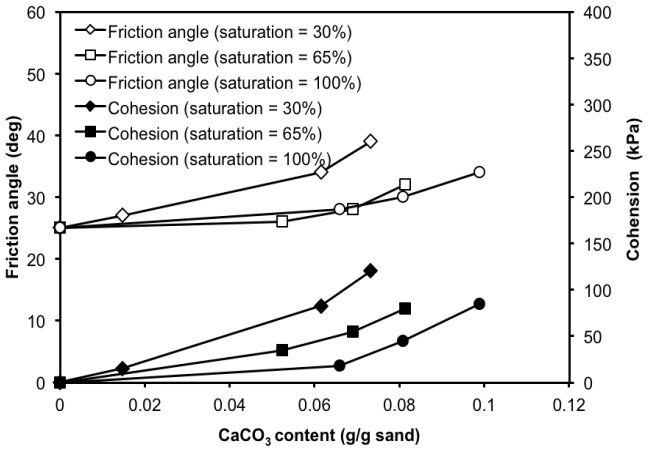
Friction angle (saturation = 30%)
Friction angle (saturation = 65%)
Friction angle (saturation = 100%)
Cohesion (saturation = 30%)
Cohesion (saturation = 65%)
Cohesion (saturation = 100%)
Friction angle (deg)
Cohension (kPa)
CaCO3 content (g/g sand)
0
10
20
30
40
50
60
0
50
100
150
200
250
300
350
400
0
0.02
0.04
0.06
0.08
0.1
0.12

Fig. 12

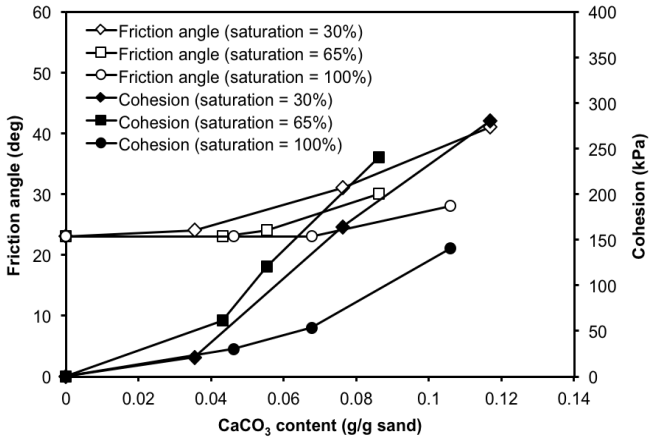
Friction angle (saturation = 30%)
Friction angle (saturation = 65%)
Friction angle (saturation = 100%)
Cohesion (saturation = 30%)
Cohesion (saturation = 65%)
Cohesion (saturation = 100%)
Friction angle (deg)
Cohesion (kPa)
CaCO3 content (g/g sand)
0
10
20
30
40
50
60
0
50
100
150
200
250
300
350
400
0
0.02
0.04
0.06
0.08
0.1
0.12
0.14

Fig. 13

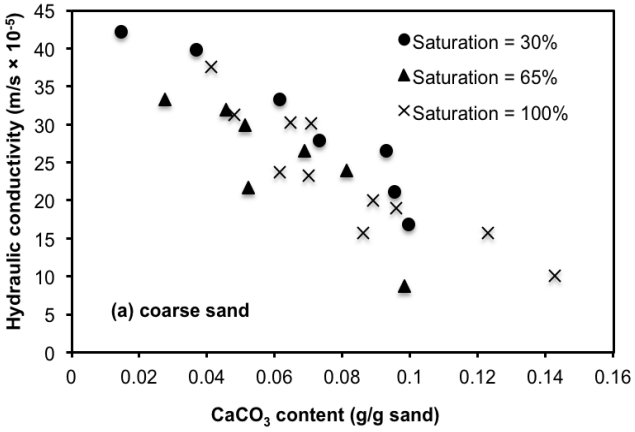
Hydraulic conductivity (m/s × 10-5)
Saturation = 30%
Saturation = 65%
Saturation = 100%
(a) coarse sand
CaCO3 content (g/g sand)

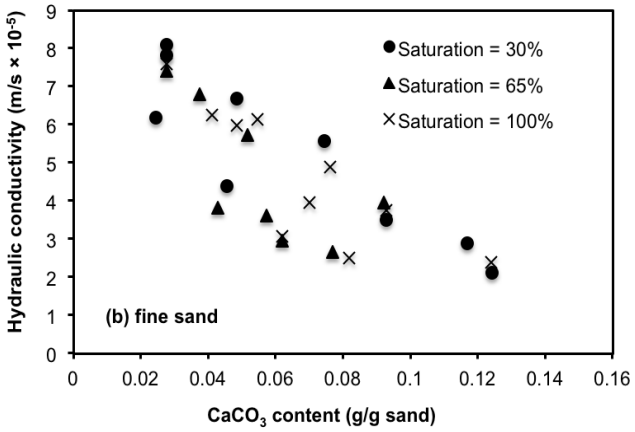
Hydraulic conductivity (m/s × 10-5)
Saturation = 30%
Saturation = 65%
Saturation = 100%
(b) fine sand
CaCO3 content (g/g sand)

Fig. 14

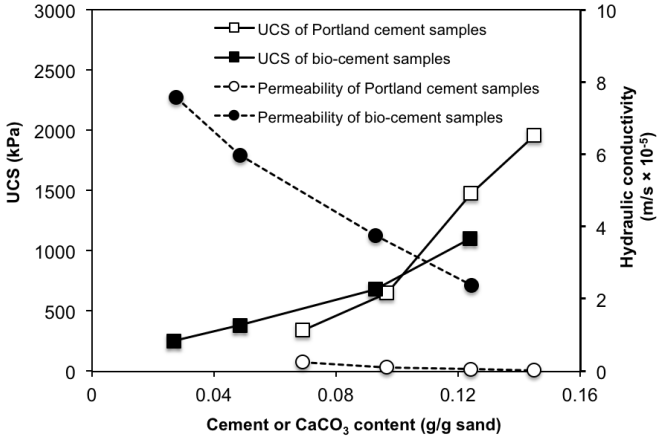
UCS of Portland cement samples
UCS of bio-cement samples
Permeability of Portland cement samples
Permeability of bio-cement samples
UCS (kPa)
Hydraulic conductivity (m/s × 10⁻⁵)
Cement or CaCO3 content (g/g sand)
3000
2500
2000
1500
1000
500
0
10
8
6
4
2
0
0
0.04
0.08
0.12
0.16

Fig. 15

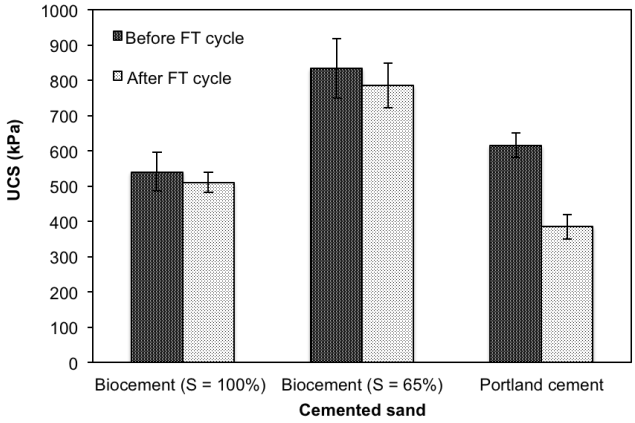
1000
900
800
700
600
500
400
300
200
100
0
UCS (kPa)
Before FT cycle
After FT cycle
Biocement (S = 100%)
Biocement (S = 65%)
Portland cement
Cemented sand

Fig. 16

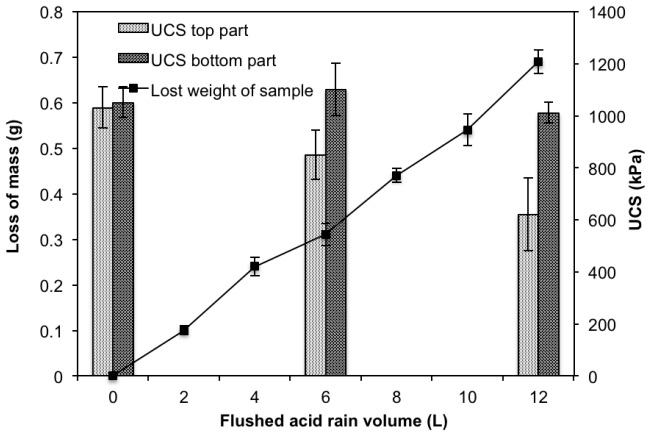
UCS top part
UCS bottom part
Lost weight of sample
Loss of mass (g)
UCS (kPa)
Flushed acid rain volume (L)
0
0.1
0.2
0.3
0.4
0.5
0.6
0.7
0.8
200
400
600
800
1000
1200
1400
0
2
4
6
8
10
12

1